Effect of Saline Waste Solution Infiltration Rates on Uranium Retention and Spatial Distribution in Hanford Sediments

Jiamin Wan[1*], Tetsu K. Tokunaga[1], Yongman Kim[1], Zheming Wang[2], Antonio Lanzirotti[3], Eduardo Saiz[4], and R. Jeffrey Serne[2]

1. Earth Sciences Division, Lawrence Berkeley National Laboratory, Berkeley, CA 94720
2. Pacific Northwest National Laboratory, Richland, WA 99352
3. University of Chicago, Chicago, IL 60637
4. Material Science Division, Lawrence Berkeley National Laboratory, Berkeley, CA 94720

ABSTRACT The accidental overfilling of waste liquid from tank BX-102 at the Hanford Site in 1951 put about 10 metric tons of U(VI) into the vadose zone. In order to understand the dominant geochemical reactions and transport processes occurred during the initial infiltration and help understand current spatial distribution, we simulated the waste liquid spilling event in laboratory sediment columns using synthesized metal waste solution. We found that, as the plume propagating through sediments, pH decreased greatly (as much as 4 units) at the moving plume front. Infiltration flow rates strongly affect U behavior. Slower flow rates resulted in higher sediment-associated U concentrations, and higher flow rates (≥ 5 cm/day) permitted practically unretarded U transport. Therefore, given the very high K_{sat} of most of Hanford formation, the low permeability zones within the sediment could have been most important in retaining high concentrations of U during initial release into the vadose zone. Massive amount of colloids, including U-colloids, formed at the plume fronts. Total U concentrations (aqueous and colloid) within plume fronts exceeded the source concentration by up to 5-fold. Uranium colloid

formation and accumulation at the neutralized plume front could be one mechanism responsible for highly heterogeneous U distribution observed in the contaminated Hanford vadose zone.

Introduction

DOE's Hanford Site is one of the most contaminated nuclear facilities in North America. The tank BX-102 overfilling event in 1951 was reported as the largest and deepest migration of U isotopes in the B-BX-BY Waste Management Area. An estimated 10 tons of U(VI) was discharged into the vadose zone as the result of this single event (1,2). A U plume has been found in the groundwater, north and east of the BX tank farm. Isotopic analyses indicate the U could have originated from this 1951 leakage (3,4). Recently, a high concentration U plume (U ≈ 0.027 M) was detected within the deep vadose zone (80 m) close to the water table, and believed to originate from the BX-102 overfill event (5), suggesting U(VI) is continuing to migrate. The DOE's remediation strategies including long-term stewardship and monitored natural attenuation need to be based on the best understanding of current U spatial distribution, speciation, and future mobility. Gaining the needed understanding is extremely difficult because of the complexity of the strongly coupled hydrological and geochemical processes, sediment heterogeneity, and insufficient historical records. Despite these difficulties, significant progress has been made during the past a few years. Studies conducted on borehole sediment samples collected from beneath BX-102 release site have provided valuable information on U fate and transport in this plume (6). A U solid phase determined to be within the uranyl silicate (uranophane) group, precipitated within microfractures of quartz and feldspar grains, based on X-ray absorption spectroscopy and X-ray diffraction (7), micro-XANES spectroscopy (8), and laser fluorescence spectroscopy (9). Slow dissolution kinetics of these U(VI) silicates from micro-

47 pores within sediment grains and intragranular mass transfer limitations is expected to keep rates
48 of U(VI) release into pore waters very low (10). The intragranular porosity and internal surface
49 area in Hanford sediments is so large that it accounts for most of the moisture and solute storage
50 capacity at the low water contents typical of the Hanford vadose zone (11), and may be effective
51 in immobilizing U(VI) (8). Laser fluorescence speciation of U in pore waters from core samples
52 indicate predominance of $UO_2(CO_3)_3^{4-}$ and $Ca_2UO_2(CO_3)_3^0$ (12). In order to study waste stream-
53 sediment reactions and plume geochemical evolution, a plume profiling method was introduced
54 (13), that is capable of providing chemical and physical properties of both pore fluid and
55 sediment at any desired location along a plume.

56 One of the most challenging issues in predicting U fate and transport is to understand the
57 dominant geochemical processes occurred during the initial infiltration of the waste solution into
58 the vadose zone sediment. These early stage processes may have largely determined the current
59 spatial distribution, speciation, and mobility of U. This study is designed to address this issue
60 through laboratory simulations of the Tank BX-102 overfilling event using the column profiling
61 method. We synthesized the waste solution (the solution that was sent to Tank BX-102) based on
62 recipe from historical records. Uncontaminated representative Hanford vadose zone sediment
63 was used to pack the columns. The experimental temperature was controlled at 70˚C to simulate
64 the field condition that was heated by radioactive decay. Because flow rates of the waste stream
65 infiltrating into the sediments are unknown and not possible to obtain directly, we chose flow
66 rate as the main variable in this study.
67

Experimental

Metal Waste Solution. It is important to recognize that there were no direct measurements or accurate historical records of the chemical compositions of the neutralized metal waste solution (MWS) at the time of the overfill event. For the tank 241-BX-102 overfill in 1951, calculated compositions were based on solubility data for the U phosphate and carbonate solids (because part of the U in the initial neutralized MWS precipitated as U phosphate and U carbonate sludge in the tank prior to and during the accidental overfill), and based on the calculated total loss of MWS from the event. From two different reports (1,2), the calculated MWS at the time of release contained 0.114 and 0.122 M U(VI), 2.1 and 2.92 M sodium, 0.61 and 0.64 M total carbonate, respectively, and 0.53 M nitrate, 0.36 M phosphate, and 0.23 M sulfate, and had pH 10.4. The estimated total U loss from the event is 10 metric tons (1,2). We took an experimentally-based approach to synthesize the MWS by going through the historical Pu extraction procedure (excluded the fission products) presented in Serne et al. (14) to obtain an approximate equilibrium partitioning of U between sludge and supernatant. Four steps were involved including metal U storage solution preparation, bismuth phosphate precipitation, centrifugation, and neutralization. After separation of precipitates and neutralizing the liquid phase to the desired pH of 10.4, the final synthesized neutralized MWS contained 0.114 M U, 0.75 M total C, 0.34 M P, 0.24 M SO_4^{2-}, 0.87 M NO_3^-, and 3.4 M Na^+, and had a pH of 10.4 (all values measured). Assuming that 0.34 M of C is associated with U as $UO_2(CO_3)_3^{4-}$, that the remaining C occurs as HCO_3^- and CO_3^{2-} in a 0.8:1 ratio at pH 10.4, and HPO_4^{2-} is the dominant P species, the total analyzed anion versus cation charge concentrations are -3.1 M_c and +3.4 M_c, respectively. These calculations do not account for the effect of high ionic strength on pK_a values

of carbonate and phosphate. The synthesized MWS was stable at both room temperature and 70˚C over the entire period of experimental time.

Sediment. Uncontaminated Hanford formation "coarse sand" was used to pack the columns. This glaciofluvial sediment was collected from the 200 East Area at a depth of about 1.5 to 3 m. Its major components are feldspar, quartz, and basaltic rock fragments. The sediment used in this study contains 93% sand, 6.0% silt, and 1.0% clay. The median grain-size is 350 μm. Calcium carbonate comprises 1.1% of the total mass. The pH measured from a sediment water extract (water to sediment mass ratio = 1:1, at 21˚C for 24 hours) was 8.4.

Column Profiling Method. The waste plume formed from the liquid overfilling event was simulated in the laboratory using the column profiling method. Waste solution seepage was simulated in sediment columns that were sectioned after plume migration to a desired distance. Columns used in this study were 0.50 meter long, constructed from 38 mm ID Teflon pipe. Uncontaminated Hanford formation sediment (at the field moisture content of 7.0 mass %) was used to pack the columns homogeneously (dry bulk density ≈ 1.65 g cm^{-3}). Column experiments were conducted at 70±0.5˚C (the estimated elevated temperature caused by decay of other radioactive isotopes not included in our MWS). Three different flow rates were used; 25, 5, and 1 cm day^{-1} (pore water velocity). The MWS was injected into the vertically oriented columns, with upward flow in order to avoid gravity induced finger flow. Solutions were supplied using syringe pumps (Harvard Apparatus), with the influent line immersed in the temperature-controlled water bath for thermal equilibration. Flow was terminated at about 30 cm of travel distance before the MWS reached the column outlet in order to capture the entire length of the simulated plume. The

113 column was quickly sectioned, and pore liquids were immediately vacuum extracted through a
114 filter for each sediment segment. Cellulose filter paper of 2µm pore size was selected because it
115 permitted rapid filtration. The extracted pore liquids were then used for a variety of analyses.
116 After the extraction, the residual pore liquid was removed from the sediment by applying 20 mL
117 distilled water evenly on the top of the drained sediment (still sitting on the filter paper under
118 vacuum extraction). This procedure for removing pore liquid from each segment took about 2
119 minutes. The sediment segments were then air-dried and used for analyses of the retained
120 amount of U. Analyses of the segment samples of extracted plume liquid and solid sediment
121 permitted construction of chemical profiles along U waste plume paths.
122
123 **Flow Rate Consideration**. Given the importance of pore water velocity on reactive transport,
124 flow rate was a key variable in this study. In many environments, the saturated hydraulic
125 conductivity, K_{sat}, of the sediment provides a reasonable upper limit for waste infiltration rates.
126 However, given the very high K_{sat} of some Hanford formation sands (10^2 to 10^4 m day^{-1}), waste
127 solution seepage probably occurred at lower rates controlled by lower permeability inter-layers
128 and by supply (leakage) rates. Information on the flow rate during the release was not attainable,
129 and to our knowledge, no attempts have been made previously to understand the flow rate effects
130 on U transport through Hanford sediments. Although our tested flow rates (25, 5, and 1 cm day^{-1})
131 only covered the slower range, results from their general trends can provide useful information.
132
133 **Analytical Methods.** The turbidity and pH of each sediment segment's pore liquid were
134 measured immediately following column sectioning and solution extraction. At the same time,
135 two fractions of each segment pore liquid (including suspended colloids if present) were

withdrawn into the prepared carrying solutions for U concentration analyses using KPA-11A (Chemchek, Richland, WA), and for other major elemental analyses using ICP. Carbon was analyzed using a TIC-TOC analyzer (O-I Analytical). The segmented sediment samples were analyzed for U content by gamma spectrometry (Gamma Table Detector, GMX-50220-P, EG&G. Ortec). Morphology, chemical composition, and structure of the colloids in plume front liquid phase were characterized using scanning electron microscopy (SEM), energy-dispersive X-ray spectrometry (EDS), and synchrotron micro-X-ray diffraction (μXRD) conducted at beamline X26A of the National Synchrotron Light Source. Uranium species in reacted sediment were determined using time-resolved laser fluorescence spectroscopy (TRLFS) conducted at the Environment Molecular Sciences Laboratory (12,15).

Results and Discussion

The results presented in this paper are mainly from three columns with three different infiltration flow rates of the synthesized MWS. An additional column run was conducted at the 25cm d^{-1} flow rate. However, only U concentration and pH values of the solution phase were analyzed. Additional repetitions were not possible because of expenses associated with synthesizing more MWS.

Plume pH Evolution and Colloid Formation

Accumulation of massive quantities of bright yellow colloids was observed in a very narrow vertical region within the extracted plume liquid phase for columns with higher flow rates ($\geq$ 5cm d^{-1}). Figure 1a is a photograph showing this phenomenon. Each vial contains the extracted liquid in its original order along a plume path. On this figure the flow direction corresponds to the sequence from right to left; displaced native pore water (initial moisture 7.0

159 mass %), plume front, and plume body. Coincident with the location of colloid accumulation,
160 dramatic pH reduction was measured within the plume front region. Figure 1b shows measured
161 plume pH profiles. The pH measurements were performed immediately after extraction of pore
162 solutions, and found to be stable upon later re-measurement. The degree of pH decrease at the
163 plume front was greater at higher flow rate. The pH decreased to as low as 6.4, four units lower
164 than the pH of initial waste solution (pH 10.4), and two units lower than pH value of the native
165 sediment pore water (pH 8.4). The measured pH values of the displaced native soil water were in
166 the range of 7.4 to 8.4 caused by different degrees of diffusive mixing with the more acidic
167 plume front liquid. For the lowest flow rate of 1.0 cm d^{-1}, the sharp pH minimum was lacking,
168 and the front exhibited only a zone of diffusely reduced pH. The longer residence times
169 associated with slower flow rates allowed diffusive mixing to diminish the sharpness of the
170 reaction front. The pH of plume bodies decreased from values near those of the influent at the
171 entry point toward neutral values at the plume front. Because U solubility is least at circum-
172 neutral pH, the pH reduction phenomenon at the advancing plume front must have driven U
173 precipitation (discussed later). Sodium concentration profiles (normalized to the inlet Na
174 concentration of 3.4 M in the MWS) are presented in Figure 1c. Sodium, as the dominant cation
175 in the very saline influent MWS, is a secondary indicator for the extent of the waste plume, but
176 its profile lags behind the plume front primarily because of portioning onto cation exchange sites.
177 In Figure 1c we see that the plume body has normalized Na concentrations close to one; a plume
178 front region has normalized Na concentrations between zero to one; and a region of displaced
179 native soil water has normalized Na concentrations close to zero. Turbidity values (Figure 1d) are
180 indicators of relative concentrations of suspended colloids. Sharp and high turbidity peaks
181 appeared at the plume front, with the peak values reaching as high as 10,000 nephelometric

turbidity units (NTU). The turbidity peaks do not precisely coincide with the pH minima. Instead, the turbidity maxima reproducibly occurred slightly behind the pH minima. In Figure 1a, the pH of bright yellow colloid-rich vial is 7.5, and its normalized Na concentration is 0.55. The pH minimum of 6.4 is associated with the adjacent downstream sample.

The degree of pH decrease and the extent of colloid formation at the plume front are both strongly depend on flow rate. Increased flow rate resulted in larger extent of pH decrease, higher degree of colloid formation, and more U accumulation at the plume front. The general mechanisms for pH decrease and colloid formation at the plume front during infiltration of high salinity solutions were discussed in earlier papers (13,16,17). In brief, it consists two processes. One is cation exchange, with Na^+ as the dominant cation rapidly and completely displacing exchangeable Ca^{2+} and Mg^{2+} from the sediment. As the plume advances, concentrations of these divalent cations build up at the plume front. Greater accumulation of these divalent cations occurs with longer distances of plume migration. The second process is precipitation of supersaturated Ca^{2+}/Mg^{2+}-bearing minerals resulting in the observed colloid formation. At the same time, precipitation reactions release protons and drive pH reduction. The pH decrease coincides with greatly decreased solubility of U(VI) minerals (18), hence also drives precipitation of U(VI) colloids.

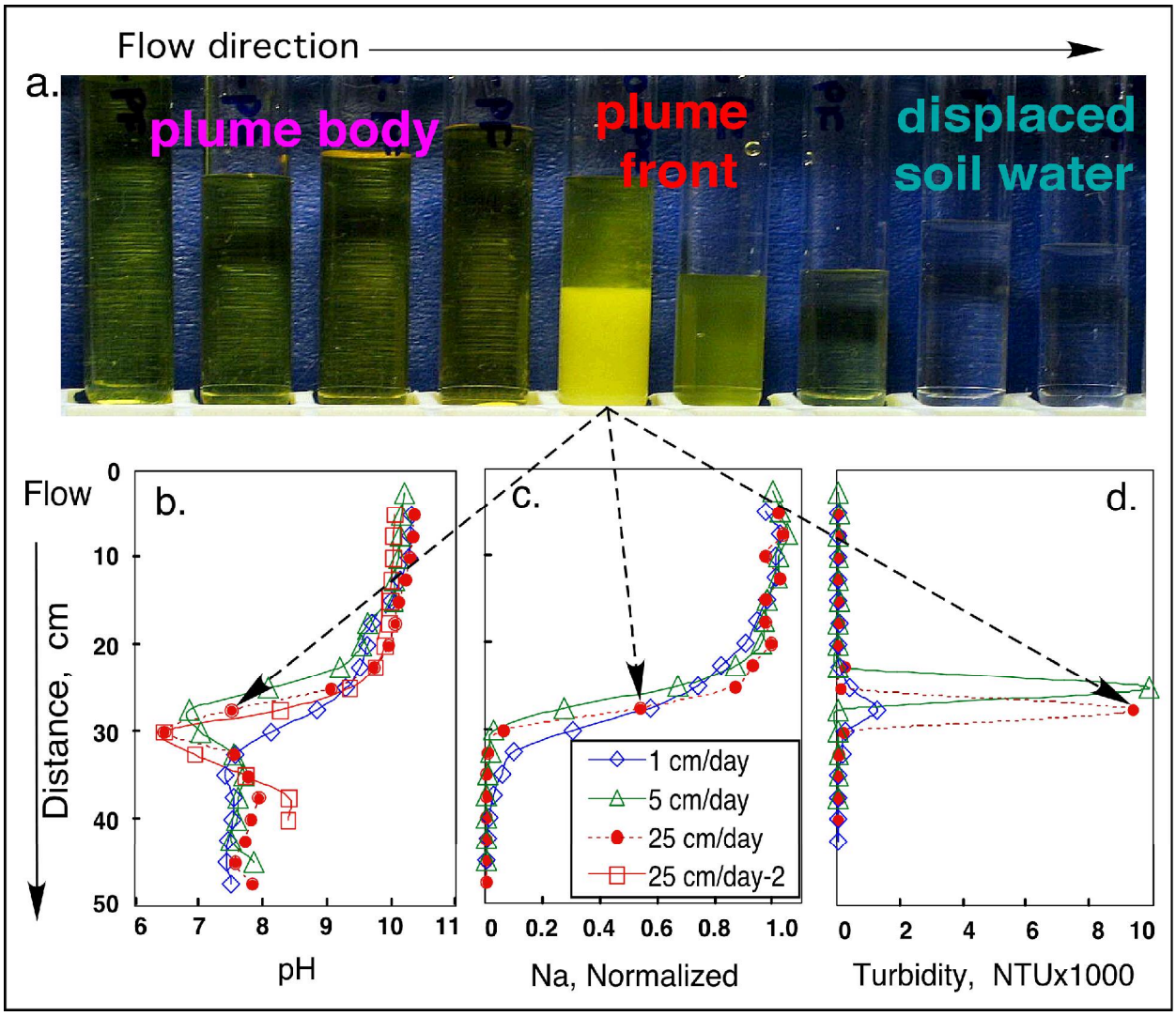

Figure 1. Plume liquid phase properties along the plume flow path. (**a.**) Photograph of extracted pore liquid from individual sections of a sediment column, showing large quantity of U-containing colloids formed at a narrow distance at the plume front. (**b.**) Plume pH profiles, showing large pH decrease at the plume fronts. (**c.**) Sodium concentration profiles. Indicating vertical distances, the plumes traveled. (**d.**) Turbidity profiles, showing high turbidity peaks occurred near the plume fronts.

211 **Major Chemical Compositions in Plume Liquid Phase**

212 The elements Na, K, Ca, Mg, P, and S were analyzed using ICP, with 5% to 10% relative
213 uncertainties determined through duplicated or triplicate runs. The C (carbonate, bicarbonate)
214 concentrations were analyzed using a TIC-TOC analyzer, also with 5-10 % uncertainties
215 determined through duplicated or triplicate runs. The element profiles of extracted plume liquids
216 are presented in Figures 2. Physical distances along the downward flow direction have been
217 normalized to the plume length, defined by the locations of the pH minima (Figure 1b), in order
218 to compensate for small variations in actual plume lengths, and to facilitate comparisons among
219 the different flow rates. Additionally, the measured major anions were normalized to their
220 influent concentrations for easier comparison between initial and reacted concentrations. Because
221 Ca, Mg, Al, and K were not contained in the influent MWS, and came solely from the sediment,
222 their measured concentrations are presented without normalization.

223 The concentration profiles of P, C, and S (the least reactive NO_3^- was not measured) are
224 presented in Figures 2-P, C, and S. Concentrations of HPO_4^{2-} decreased rapidly with depths, and
225 showed greatest loss from solution at the lowest flow rate. For example, at 25 cm of infiltration
226 distance the MWS lost 70% and 35% of its initial HPO_4^{2-} under infiltration rates of 1 and 25 cm
227 d^{-1}, respectively. Theses losses indicate rapid phosphate precipitation occurred during MWS
228 infiltration. Carbonate profiles show normalized values close to 1.0, and increase with increased
229 depths for two columns, indicating little carbonate loss during reactions. We do not know why C
230 concentrations increase with distance. Sulfate behaved very differently. The SO_4^{2-} profiles were
231 fairly uniform throughout most of the pore solution profiles, with up to about 5% loss from the
232 influent concentration (Figure 5-S.). However, sharp and high SO_4^{2-} peaks (normalized S up to
233 1.6 for the highest flow rate) appeared just behind the plume fronts. The SO_4^{2-} concentration peak

234 was not present under slowest flow rate. Recall that the extracted pore solutions were filtered
235 through 2 μm membranes, which would remove only the larger suspended colloids. A possible
236 mechanism for SO_4^{2-} accumulation just behind the plume front is homogeneous precipitation of
237 SO_4^{2-}-containing gypsum colloids within the Ca-rich plume front. The small lag of the SO_4^{2-}
238 peak relative to that of the plume front Ca^{2+} peak may have resulted from slight retardation of
239 newly formed particles. This possibility is supported by later measured plume front colloids
240 containing dominantly S and Ca using SEM EDS.

241 Sharp peaks of Ca^{2+} and Mg^{2+} were detected at the plume fronts, with concentrations up
242 to hundreds of mM for Ca^{2+} and tens of mM for Mg^{2+} (Figures 2-Ca, Mg). These divalent
243 cations accumulated from Na^+ replacing exchangeable Ca^{2+} and Mg^{2+} from the mineral surfaces
244 of the sediment. The cation exchange capacities for coarse and fine Hanford sands have been
245 reported in the range of 17 to180 $mmol_c\ kg^{-1}$ (6). In these Hanford sands, Ca^{2+} and Mg^{2+} account
246 for about 80% and 13% of the exchangeable bases, respectively. The observed Ca^{2+}/Mg^{2+} spatial
247 distributions not only reflect rapid cation exchange, but diffusion and hydrodynamic dispersion
248 as well. Longer travel times associated with slower flow rates result in more diffuse Ca^{2+}/Mg^{2+}
249 displacement fronts (13). The enriched K^+ within the plume relative to the displaced soil water
250 resulted mainly from dissolution of K-containing minerals, although native Hanford sediments
251 do have some cation-exchangeable K^+ (Figure 2-K). The broadness of the K^+-enriched region
252 and its lag behind the sharp Ca^{2+} and Mg^{2+} peaks, reflect slower kinetics of K^+ release through
253 mineral dissolution relative to rapid cation exchange.
254

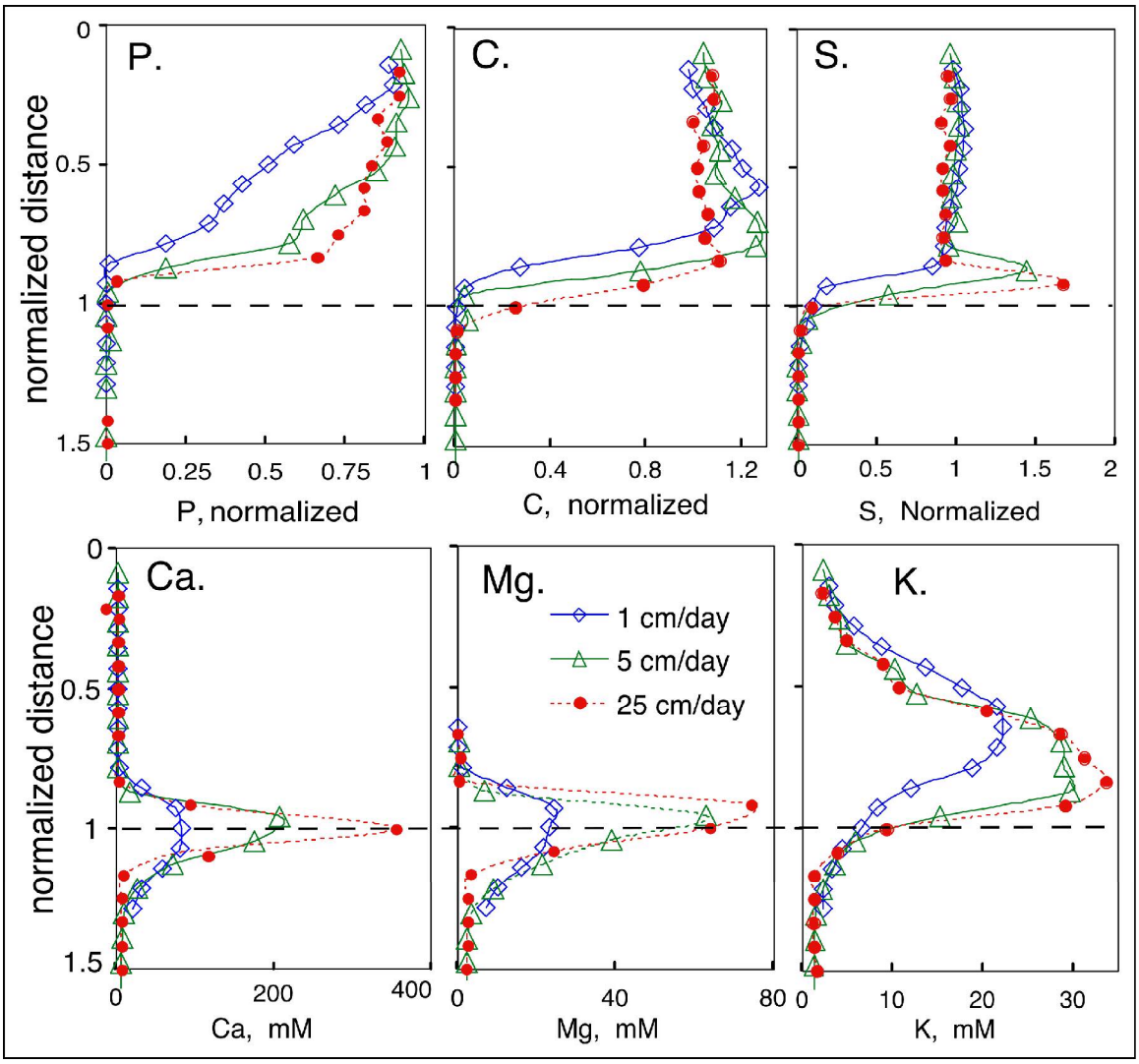

255

256 **Figure 2.** Concentration profiles of some major ions in the plume liquid phase. The measured
257 concentration for P, C, and S were normalized to their influent concentrations (0.34M P, 0.75M
258 C, and 0.24M S) in the initial MWS. The initial MWS did not contain Ca, Mg, and K, and their
259 only source is the sediment.

260

261 **U Spatial distribution within a plume**

262 The uncertainties in U concentration data were 3-5% for liquid phase analyses using
263 KPA, and ~20% for sediment using gamma ray spectrometry (triplicates). In the plume body

region (Figure 3a), normalized U profiles are close to and slightly reduce from unity for the 5 and 25 cm d^{-1} flow rates, showing at most about 5% lose of U from the original MWS. This U depleted from plume body liquid was adsorbed by sediment. For the sediment column infused at 1 cm d^{-1}, normalized U values are ≤ 0.25, indicating >75% of U was retained by the sediment.

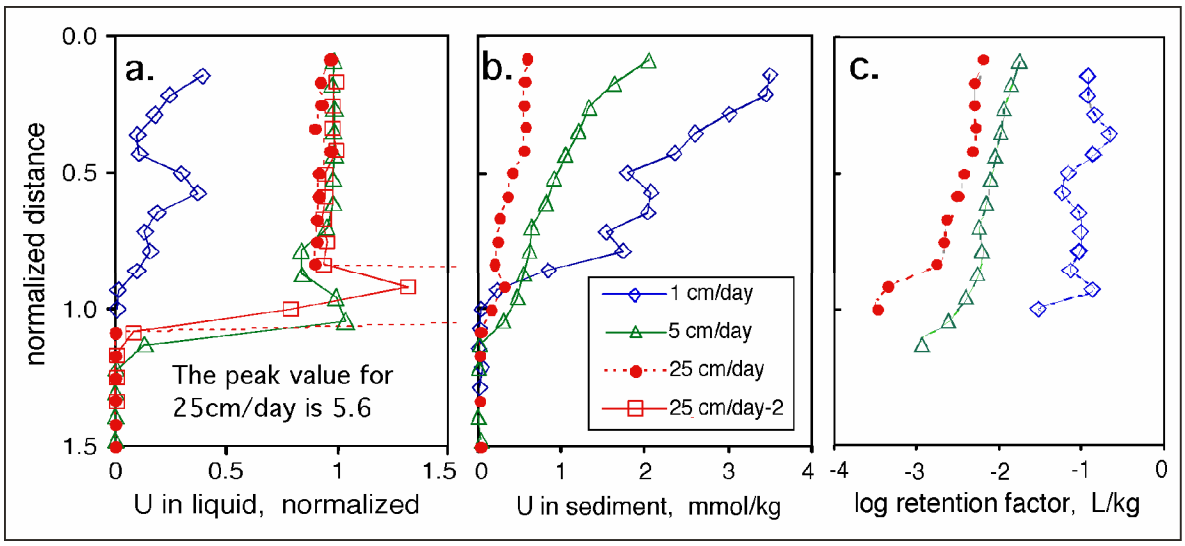

Figure 3. Spatial distribution of U within a plume, showing flow rate effects. (**a.**) U concentration profiles in pore liquid phase normalized to the influent U concentration in the MWS, showing U accumulation at the plume front region under higher flow rates. (**b.**) U concentration profiles in the sediment solid phase, and (**c.**) U ratios of solid-associate U to solution U, presented as profiles of $\log_{10}$ retention factor.

The absolute concentrations of elements in the plume front are highly variable because of their steep concentration gradients associated with being within a moving reaction front. For example, in the 5 cm d^{-1} column, measured geochemical parameters within one of the plume front segments included pH 7.0, U 124 mM, C 193 mM P 0.2 mM, and S 18 mM. These

280 concentrations are especially transient under rapid flow conditions. If samples were taken at
281 slightly different locations or times, or by using a different filter pore size, different
282 concentrations of these elements would probably have been obtained. However, the data convey
283 the basic message that most of the plume front U was not in complexes with either P or S. More
284 interestingly, from C:U ratio of 1.6 in this particular plume front sample, much of its U was no
285 longer in complexes with carbonate [$UO_2(CO_3)_3^{-4}$]as it was originally in the MWS. When the
286 solution pH dropped from 10 to 7.0, U(VI) solubility drops to ~10^{-5} M (e.g., schoepite). Thus, the
287 plume front is a moving zone within which the advancing U precipitates. The fact that
288 suspension U concentrations exceed that of the source solution under higher flow rates shows
289 that U precipitation is homogeneous, and that deposition of newly formed U(VI) colloids is
290 kinetically limited.

291 The flow rate-dependence of U transport at the plume front is evident in U liquid phase
292 concentration profiles (Figure 3a). Recall that finer suspended colloids are included in the
293 "solution" phase because 2 μm filters were used. The normalized U concentrations for the two
294 faster flow rate columns are greater than one in the plume front region, indicating local
295 accumulation of suspended U colloids. As mentioned earlier, only pH and liquid phase U
296 concentration data were obtained for the duplicate run 25 cm/day-2. The normalized U
297 concentrations from the second run yielded a lower peak value of 1.38 at the front (Figure 3a)
298 compared to 5.6 for run 25 cm/day-1. Although the U peak value was not quantitatively
299 reproduced, the phenomenon of U accumulation in the plume front was confirmed. As discussed
300 previously, the extremely nonequilibrium conditions make replication of U concentrations within
301 the plume front very difficult. In contrast, slower flow rates permit closer approach to local
302 equilibrium within the plume front, and no U accumulation at the plume front occurred in the 1

303 cm d^{-1} column. Thus, the extent of U transport reflects complex flow rate-dependent factors
304 including homogeneous colloid formation from highly supersaturated pore liquids, and colloid
305 deposition onto the stationary sediment matrix.

306 U concentrations retained by the sediment solid phase (through sorption and
307 precipitation) are presented in Figure 3b. The U concentrations in sediments at different flow
308 rates were generally inversely related to aqueous phase U profiles in Figure 3a. Slower flow rates
309 resulted in higher sediment-associated U concentrations, reflecting significant rate limitations to
310 sorption and precipitation. Partitioning of U within the plume between the sediment solids and
311 pore liquids was described in terms of a retention factor (L kg^{-1}), obtained by dividing the U
312 concentration measured on the solids by that measured in the associated pore waters (L/kg). The
313 retention factors shown in Figure 3c differ from the conventional retardation factor K_d in that
314 geochemical equilibrium is not assumed, and both sorbed and solid phase U are included in the
315 sediment-associated component. The retention factor is useful because it directly indicates the
316 ratio of relatively immobile U vs. still highly mobile U within the plume. These data show that
317 within the main plume bodies, retention of U in solid phases are ~1.5 order of magnitude higher
318 for the lowest flow rate relative to higher flow rate cases (Figure 3c). The fact that retention
319 factors at the plume fronts are lower, even though this region is lowest in pH and thus most
320 favorable for U sorption and precipitation, is consistent with the presence of significant quantities
321 of suspended U colloids. Kinetic limitations are reflected in the fact that the sediment at the
322 plume front has only been exposed to the U-rich MWS for short times. Note that for the 25, 5,
323 and 1 cm d^{-1} flow rates, sediments within 1 cm of the advancing front have only been exposed to
324 U for about 1, 5, and 24 hours, respectively. The high Ca^{2+} concentration within the neutral

325 plume front also drives formation of aqueous $Ca_2UO_2(CO_3)_3^0$ complexes (19-21), which
326 diminishes U sorption (21) and enhances U transport (22).
327
328 **Plume Front Colloids**
329 The plume front colloids from the 25cm d^{-1} column at the segment with pH 7.5 were
330 analyzed. SEM images presented in Figure S1a (online Supporting Information, SI) show typical
331 morphologies of the colloids. The size and morphology information suggested that further
332 growth and nucleation of colloids occurred after the pore liquid was extracted, because some
333 particles are larger than the 2 μm pore size of the filter used in the extraction. Chemical
334 compositions of the particles were analyzed qualitatively using energy-dispersive X-ray
335 spectrometry (EDS) in areas of ≥ 1 μm^2. The major elements within the colloids were identified
336 as Ca, P, U, O, Na, Mg, C, and S (Figures S1b, c, d). Synchrotron X-ray micro-diffraction
337 (μXRD) was used to characterize U-rich crystalline phases of the colloids (Figure S1e). The best
338 XRD fit was obtained with sodium uranyl carbonate $Na_4(UO_2)(CO_3)_3$. Some amorphous or very
339 finely crystalline uranyl oxyhydroxides and calcium uranyl phosphates are present in the colloid
340 phase based on the EDS data. The existence of S-containing colloids is consistent with the
341 previously described accumulation of SO_4^{2-} near the front (Figure 2S).
342
343 **U Retained by the Sediment**
344 Reacted sediment from the 1 cm d^{-1} column was chosen for this study because its
345 sediment retained highest U (Figure 3e). Samples were obtained from two locations within the
346 plume, at normalized distances 0.76 (sample 1cm-11) and 0.50 (sample 1cm-15). Without further
347 treatment, rinsed and air-dried sediment grains were used for SEM, EDS, and fluorescence

spectroscopy analyses. The SEM image shows the morphology of the secondary minerals on a grain surface (Figure S2A). The EDS spectrum (Figure S2B) provides the chemical composition of the secondary mineral(s) showing U present with other major elements. Results of laser fluorescence analyses are presented in Figures S2C-E (discussed in the online SI). Through comparison with a set fluorescence spectra of natural uranyl minerals, the spectrum of sample 1cm-15 matched that of liebigite [$Ca_2(UO_2)(CO_3)_3$]. An unique match for U species in sample 1cm-11 was not obtained because its fluorescence spectrum is similar to the spectra of two standard uranium minerals, phosphuranylite {$Ca(UO_2)[(UO_2)_3(OH)_2(PO_4)_2]_2(H_2O)_{12}$} and zellerite [$Ca(UO_2)(CO_3)_2(H_2O)_5$]. The uranium silicate species boltwoodite [$K(UO_2)(SiO_3OH)(H_2O)_{1.5}$] was absent in this sample.

Implications on Understanding Contaminant U in Hanford Vadose Zone

Several processes demonstrated in these laboratory experiments have direct relevance to U-contaminated sediments such as those at the Hanford 200 Area vadose zone. The pH within an alkaline U plume varied from its waste solution value of 10.4 at the point of discharge, down to ~7.0 at the moving front. Peaks of Ca^{2+} and Mg^{2+} concentrations appeared at the plume front as the result of rapid cation exchange from sediments (displacement by Na^+) from the infiltrating waste liquid. These results are consistent with the only available field profile data from borehole 299-E33-45 at Hanford tank 241-BX-102. The pH profile from the borehole sediment showed pH values varying from 9.6 to 7.3 downward along the flow path, and the high peak concentrations of Ca^{2+} and Mg^{2+} are also observed in the borehole profiles with a neutral pH (6). The Ca^{2+}/Mg^{2+} peaks along with neutral pH may be signatures of a plume front in the field.

The neutralized pH caused homogeneous U precipitation, and the formation of suspended U-colloids. The measured U accumulation at the plume front exceed its source level by several-fold under the highest tested flow rate. This process might have been one of the causes for the highly heterogeneous distribution of U within vadose zone waste plumes, such as that characterized by samples from borehole 299-E33-45 at the Hanford Site (6).

This work also shows that kinetic limitations on sorption and precipitation permit practically unretarded U transport at flow rates ≥ 5 cm/day. Given the very high K_{sat} of Hanford formation sands (10^2 to 10^4 m day^{-1}), the rates of the initial waste liquid seepage could easily have been higher than 5 cm d^{-1}. Therefore low permeability zones within the sediment might have been most important in slowing transport of high concentrations of U during initial release into the Hanford vadose zone. Predictions based on equilibrium K_d partitioning of U would greatly underestimate the extent of U migration.

Acknowledgments

We thank Associate Editor Janet Hering for her careful review and suggestions that made this a better paper. We also acknowledge the anonymous reviewers for their helpful comments. Experimental support by J. Larsen and Y. T. He is gratefully acknowledged. This work was carried out under U.S. Department of Energy Contract No. DE-AC03-76SF-00098. Funding was provided by the U.S. Department of Energy (DOE), Environmental Remediation Science Program (ERSP).

Supporting Information Available

Additional materials are presented in Supporting Information via the Internet, including figures

showing morphologies, chemical compositions, synchrotron micro-X-ray diffraction pattern of plume front colloids, and SEM, EDS, and fluorescence spectroscopy analyses of sediment retained U species. These information are available free of charge via the Internet at http://pubs.acs.org.

Literature Cited

(1) Jones, T. E.; Simpson, B. C.; Wood, M. I.; Corbin, R. A. Preliminary inventory estimates for single-shell tank leaks in B, BX, and BY tank farms. *CH2M Hill, Hanford Group. Inc.: Richland, WA* **2001**.

(2) Corbin, R. A.; Simpson, B. C.; Anderson, M. J.; Danielson III, W. F.; Field, J. G.; Jones, T. E.; Kincaid, C. T. Hanford soil inventory model (SIM) Rev. 1. *RPP-26744 Rev.0, CH2M HILL Hanford Group, Inc. , Richland, WA* **2005**.

(3) Christensen, J. N.; Dresel, P. E.; Conrad, M. E.; Maher, K.; Depaolo, D. J. Identifying the sources of subsurface contamination at the Hanford Site in Washington using high-precision uranium isotopic measurements. *Environmental Science and Technology* **2004**, *38*, 3330-3337.

(4) Dresel, P. E.; Evans, J. C.; Farmer, O. T. Investigation of isotopic signatures for sources of groundwater contamination at the Hanford Site. *PNNL-13763; Pacific Northwest National Laboratory: Richland, WA* **2002**.

(5) McCain, R. G. Gamma and neutron Logs of 299-E33-18. *DOE-EM/GJ1302-2006, Stoller Hanford Office, Richland, WA*. **2006**.

(6) Serne, R. J.; Last, G. V.; Gee, G. W.; Schaef, H. T.; Lanigan, D. C.; Lindenmeier, C. W.; Lindberg, M. J.; Clayton, R. E.; Legore, V. L.; Orr, R. D.; Kutnyakov, I. V.; Baum, S. R.; Geiszler, K. N.; Brown, C. F.; Valenta, M. M.; Vickerman, T. S. Characterization of vadose

416 zone sediment: Borehole 299-E33-45 near BX-102 in the B-BX-BY waste management area.
417 *PNNL-14083; Pacific Northwest National Laboratory: Richland, WA* **2002**.
418 (7) Catalano, J. G.; McKinley, J. P.; Zachara, J. M.; Heald, S. M.; Smith, S. C.; Brown, G.
419 E., Jr. Changes in uranium speciation through a depth sequence of contaminated Hanford
420 sediments. *Environmental Science and Technology* **2006**, *40*, 2517-2524.
421 (8) McKinley, J. P.; Zachara, J. M.; Liu, C.; Heald, S. C.; Prenitzer, B. I.; Kempshall, B. W.
422 Microscale controls on the fate of contaminant uranium in the vadose zone, Hanford Site,
423 Washington. *Geochimica Cosmochimica Acta* **2006**, *70*, 1873-1887.
424 (9) Wang, Z.; Zachara, J. M.; Gassman, P. L.; Liu, C.; Qafoku, O.; Catalano, J. G.
425 Fluorescence spectroscopy of U(VI)-silicate and U(VI)-contaminated Hanford sediment.
426 *Geochimica Cosmochimica Acta* **2005**, *69*, 1391-1403.
427 (10) Liu, C.; Zachara, J. M.; Qafoku, O.; McKinley, J. P.; Heald, S. M.; Wang, Z.
428 Dissolution of uranyl microprecipitates in subsurface sediments at Hanford Site, USA.
429 *Geochimica Cosmochimica Acta* **2004**, *68*, 4519-4537.
430 (11) Tokunaga, T. K.; Olson, K. R.; Wan, J. Moisture characteristics of Hanford gravels:
431 Bulk, grain-surface, and intragranular components. *Vadose Zone J.* **2003**, *2*, 322-329.
432 (12) Wang, Z.; Zachara, J. M.; Yantasee, W.; Gassman, P. L.; liu, C.; Joly, G. Cryogenic
433 laser induced fluorescence characterization of U(VI) in Hanford vadose zone pore waters.
434 *Environmental Science and Technology* **2004**, *38*, 5591-5597.
435 (13) Wan, J.; Tokunaga, T. K.; Larsen, J. T.; Serne, R. J. Geochemical evolution of highly
436 alkaline and saline tank waste plumes during seepage through vadose zone sediments.
437 *Geochimica Cosmochimica Acta* **2004**, *68*, 491-502.

(14) Serne, R. J.; Jones, T. E.; Lindberg, M. J.; Schaef, H. T.; K. M. Krupka, K. M. Laboratory Scale Bismuth Phosphate Extraction Process Simulation To Track Fate of Fission Products. *PNNL-14120, Pacific Northwest National Laboratory, Richland, WA* **2003**.

(15) Wang, Z.; Zachara, J. M.; Mckinley, J. P.; Smith, S. C. Cryogenic laser induced U(VI) fluorescence studies of a U(VI) substituted natural calcite: implications to U(VI) speciation in contaminated Hanford sediments. *Environmental Science and Technology* **2005**, *39*, 2651-2659.

(16) Wan, J.; Tokunaga, T. K.; Saiz, E.; Larsen, J. T.; Zheng, Z. Colloid formation at waste plume fronts. *Environmental Science and Technology* **2004**, *38*, 6066-6073.

(17) Wan, J.; Larsen, J. T.; Tokunaga, T. K.; Zheng, Z. pH neutralization and zonation in alkaline-saline tank waste plumes. *Environmental Science and Technology* **2004**, *38*, 1321-1329.

(18) Langmuir, D. *Aqueous Environmental Geochemistry*; Prentice-Hall: Upper Saddle River, NJ, 1997.

(19) Bernhard, G.; Geipel, G.; Reich, T.; Brendler, V.; Amayri, S.; Nitsche, H. Uranyl(VI) carbonate complex formation: Validation of the Ca2UO2(CO3)3 (aq.) species. . *Radiochimica Acta* **2001**, *89*, 511-518.

(20) Dong, W.; Brooks, S. C. Determination of the formation constants of ternary complexes of uranyl and carbonate with alkaline earth metals (Mg2+, Ca2+, Sr2+, and Ba2+) using anion exchange method. *Environmental Science and Technology* **2006**, *40*, 4689-4695.

(21) Zheng, Z.; Tokunaga, T. K.; Wan, J. Influence of calcium carbonate on U(VI) sorption to soils. *Environ. Sci. Technol* **2003**, *37*, 5603-5608.

(22) Tokunaga, T. K.; Wan, J.; Pena, J.; Sutton, S. R.; Newville, M. Hexavalent uranium diffusion into soils from concentrated acidic and alkaline solutions. *Environmental Science and Technology* **2004**, *38*, 3056-3062.

461

462

463 **Brief**

464 Infiltration flow rates of uranium-rich, saline waste solution strongly affect uranium retention

465 and spatial distribution within the Hanford vadose zone sediments.